A Voltage and Frequency Droop Control Method for Parallel Inverters

Karel De Brabandere, *Student Member, IEEE*, Bruno Bolsens, *Student Member, IEEE*, Jeroen Van den Keybus, *Student Member, IEEE*, Achim Woyte, Johan Driesen, *Member, IEEE*, and Ronnie Belmans, *Fellow, IEEE*

***Abstract*—In this paper, a new control method for the parallel operation of inverters operating in an island grid or connected to an infinite bus is described. Frequency and voltage control, including mitigation of voltage harmonics, are achieved without the need for any common control circuitry or communication between inverters. Each inverter supplies a current that is the result of the voltage difference between a reference ac voltage source and the grid voltage across a virtual complex impedance. The reference ac voltage source is synchronized with the grid, with a phase shift, depending on the difference between rated and actual grid frequency. A detailed analysis shows that this approach has a superior behavior compared to existing methods, regarding the mitigation of voltage harmonics, short-circuit behavior and the effectiveness of the frequency and voltage control, as it takes the R to X line impedance ratio into account. Experiments show the behavior of the method for an inverter feeding a highly nonlinear load and during the connection of two parallel inverters in operation.**

***Index Terms*—Autonomous power systems, converter control, dispersed generation, finite output-impedance ac voltage source emulation, frequency and voltage droops, harmonics, parallel connection, power quality, microgrids, stand-alone systems, uninterruptible power supplies (UPS), virtual impedance, voltage source inverter, mixed voltage-current control.**

I. Introduction

FREQUENCY and voltage control in island grids or uninterruptible power supplies (UPS) systems, supplied by several inverters in parallel, can be obtained using various control methods, either with or without communication. Control methods solely based on local measurements exhibit a superior redundancy, as they do not rely on communication for reliable operation. A peculiar aspect of these methods is that they only have a proportional controller for frequency and voltage, lacking any form of integral control. Control of a distributed system without communication can only be achieved at the price of permitting a small error. Therefore, these techniques are generally denoted as droop control methods [1]–[13]. The small droop is generally considered acceptable as long as the error remains within predefined limits. However, if desired, the local droop control could be extended by a global integral control through low bandwidth communication [1], combining both redundancy and integral control. In this paper, only the local droop control, without communication, is elaborated. The global integral control may be regarded as a possible, though not necessary, extension.

This paper starts with a review of the droop control method. Although this method performs well for inductive lines, the performance in case of resistive lines is poor. In this paper, it is shown how the classical droop method can easily be adapted to account for the grid impedance, providing good performance under all conditions. A major benefit of this technique is especially prevalent in low-voltage cable grids, generally having a mainly resistive line impedance. In these grids, the proposed technique is appreciably more efficient in controlling frequency and voltage in proportion to the needed active and reactive power flows, as it takes the X over R ratio of the line impedance into account. Second, it is explained why the approach of controlling active and reactive current instead of active and reactive power exhibits some advantages, especially in case of a short circuit. Controlling any non-zero active or reactive power during short circuit (grid voltage equals zero) results in infinitely high currents, which is avoided when controlling the active and reactive current directly. Finally, a time-domain approach to obtain voltage and frequency droop control is described. A complex finite-output impedance voltage source is imitated, by controlling the current, flowing through a virtual impedance as a result of the voltage difference between a virtual ac source and the grid. In contrast to the classical droop control, the presented approach inherently controls not only the fundamental voltage and frequency, but also the harmonic components of the voltage, and is therefore suited to supply highly nonlinear loads. A detailed analysis shows that, with exception of the additional harmonic control, the performance of this new approach is equivalent to the abovementioned droop control through controlling active and reactive current.

Manuscript received September 9, 2004; revised May 30 2006. This work was supported in part by the Belgian IWT-GBOU research project on embedded generation and in part by the European Commission FP5 Dispower project ENK5-CT2001-00522. This paper was presented at the Power Electronics Specialists Conf. (PESC), Aachen, Germany, June 20–25, 2004. Recommended for publication by Associate Editor J. Kolar.

K. De Brabandere, B. Bolsens, J. Van den Keybus, J. Driesen, and R. Belmans are with the Katholieke Universiteit Leuven, Department ESAT/ELECTA, B-3001 Leuven, Belgium (e-mail: Ronnie.belmans@esat.kuleuven.be).

A. Woyte is with Policy Studies Department, 3E S.A., B-1000 Brussels, Belgium.

Digital Object Identifier 10.1109/TPEL.2007.900456

II. Theoretical Background

A. Droop Control Through Active and Reactive Power

The power flowing into a line at point A, as represented in Fig. 1, is described [14]

$$\begin{aligned} P + jQ = \underline{S} = \underline{U}_1 \underline{I}^* &= \underline{U}_1 \left(\frac{\underline{U}_1 - \underline{U}_2}{\underline{Z}} \right)^* \\ &= U_1 \left(\frac{U_1 - U_2 e^{j\delta}}{Z e^{-j\theta}} \right) \\ &= \frac{U_1^2}{Z} e^{j\theta} - \frac{U_1 U_2}{Z} e^{j(\theta+\delta)}. \end{aligned} \tag{1}$$

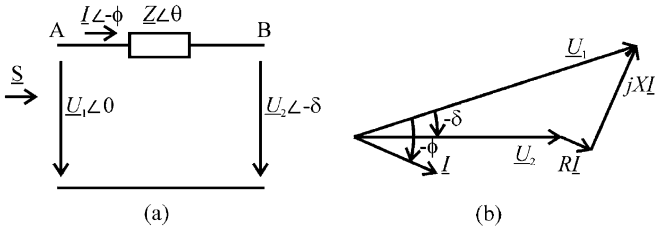

Fig. 1. (a) Power flow through a line and (b) phasor diagram.

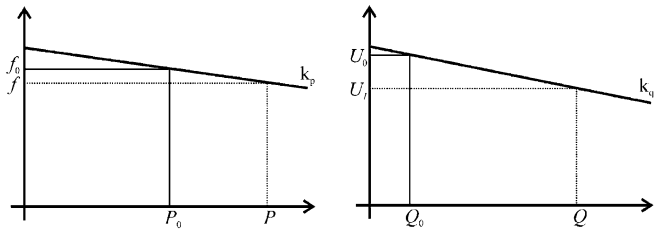

Fig. 2. frequency and voltage droop control characteristics.

Thus, the active and reactive power flowing into the line are

$$P = \frac{U_1^2}{Z}\cos\theta - \frac{U_1 U_2}{Z}\cos(\theta+\delta) \tag{2}$$

$$Q = \frac{U_1^2}{Z}\sin\theta - \frac{U_1 U_2}{Z}\sin(\theta+\delta). \tag{3}$$

With $Ze^{j\theta} = R + jX$, (2) and (3) are rewritten as

$$P = \frac{U_1}{R^2+X^2}[R(U_1 - U_2\cos\delta) + XU_2\sin\delta] \tag{4}$$

$$Q = \frac{U_1}{R^2+X^2}[-RU_2\sin\delta + X(U_1 - U_2\cos\delta)] \tag{5}$$

or

$$U_2\sin\delta = \frac{XP - RQ}{U_1} \tag{6}$$

$$U_1 - U_2\cos\delta = \frac{RP + XQ}{U_1}. \tag{7}$$

For overhead lines $X \gg R$, which means that R may be neglected. If also the power angle δ is small, then $\sin\delta = \delta$ and $\cos\delta = 1$. Equations (6) and (7) then become

$$\delta \cong \frac{XP}{U_1 U_2} \tag{8}$$

$$U_1 - U_2 \cong \frac{XQ}{U_1}. \tag{9}$$

For $X \gg R$, a small power angle δ and voltage difference $U_1 - U_2$, (8) and (9) show that the power angle depends predominantly on P, whereas the voltage difference depends predominantly on Q. In other words, the angle δ can be controlled by regulating P, whereas the inverter voltage U_1 is controllable through Q. Control of the frequency dynamically controls the power angle and, thus, the real power flow. Thus, by adjusting P and Q independently, frequency and amplitude of the grid voltage are determined. These conclusions form the basis for the well-known frequency and voltage droop regulation through respectively active and reactive power

$$f - f_0 = -k_p(P - P_0) \tag{10}$$

$$U_1 - U_0 = -k_q(Q - Q_0) \tag{11}$$

f_0 and U_0 are rated frequency and grid voltage respectively, and P_0 and Q_0 are the (momentary) set points for active and reactive power of the inverter. The frequency and voltage droop control characteristics are shown graphically in Fig. 2.

As a first improvement to the control scheme, R is no longer neglected. This is key in low voltage cable grids, generally having a mainly resistive line impedance. Ultimately, X could be neglected instead of R. In this case, adjusting active power P influences the voltage amplitude, while adjusting reactive power Q influences the frequency. Relationships have changed radically, in such a way that the droop regulation described by (10) and (11) is no longer effective.

In the general case, both X and R are to be considered. Then, the use of an orthogonal linear rotational transformation matrix T from active and reactive power P and Q to the "modified" active and reactive power P' and Q' is proposed

$$\begin{bmatrix} P' \\ Q' \end{bmatrix} = \mathbf{T}\begin{bmatrix} P \\ Q \end{bmatrix} = \begin{bmatrix} \sin\theta & -\cos\theta \\ \cos\theta & \sin\theta \end{bmatrix}\begin{bmatrix} P \\ Q \end{bmatrix} = \begin{bmatrix} \frac{X}{Z} & -\frac{R}{Z} \\ \frac{R}{Z} & \frac{X}{Z} \end{bmatrix}\begin{bmatrix} P \\ Q \end{bmatrix}. \tag{12}$$

Applying this transformation on (4) and (5) results in

$$\sin\delta = \frac{ZP'}{U_1 U_2} \tag{13}$$

$$U_1 - U_2\cos\delta = \frac{ZQ'}{U_1}. \tag{14}$$

For a small power angle δ and voltage difference $U_1 - U_2$, (13) and (14) show that the power angle depends only on P', whereas the voltage difference depends only on Q'. In other words, the angle δ can be controlled by regulating P', whereas the inverter voltage U_1 is controllable through Q'. As the grid frequency is influenced through the angle δ, the definition of P' and Q' permits to independently influence the grid frequency and amplitude. This is illustrated graphically in Fig. 3. The effect of P', Q', P, and Q on voltage and frequency is illustrated for different ratios of R/X. To derive P' and Q', it suffices to know the ratio R/X. Knowledge of the absolute values of the line impedance is not needed ($\varphi = \pi - \theta = \operatorname{atan}(R/X)$).

From Fig. 3, it can be seen that for mainly inductive lines $P' \cong P$ and $Q' \cong Q$, whereas for mainly resistive lines $P' \cong -Q$ and $Q' \cong P$. Hence, the frequency and voltage droop regulation becomes

$$f - f_0 = -k_p(P' - P_0') = -k_p\frac{X}{Z}(P - P_0) + k_p\frac{R}{Z}(Q - Q_0) \tag{15}$$

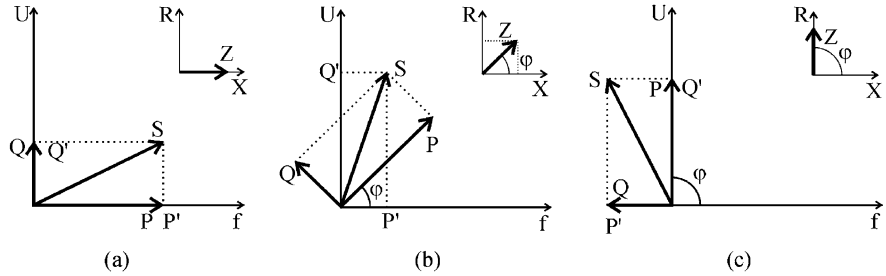

Fig. 3. Influence of active and reactive power on voltage and frequency for different line impedance ratios: (a) $\mathrm{R/X} = 0$, (b) $\mathrm{R/X} = 1$, (c) $\mathrm{R/X} = \infty$.

$$U_1 - U_0 = -k_q(Q' - Q'_0) = -k_q\frac{R}{Z}(P - P_0) - k_q\frac{X}{Z}(Q - Q_0). \quad (16)$$

B. Droop Control Through Active and Reactive Current

Active and reactive current I_a and I_r through $\underline{Z}$ are

$$I_a = \frac{P}{U_1} = \frac{R(U_1 - U_2\cos\delta) + XU_2\sin\delta}{R^2 + X^2} \quad (17)$$

$$I_r = \frac{Q}{U_1} = \frac{-RU_2\sin\delta + X(U_1 - U_2\cos\delta)}{R^2 + X^2}. \quad (18)$$

Then, analogous to the modified active and reactive power, modified active and reactive current are defined as

$$\begin{bmatrix} I'_a \\ I'_r \end{bmatrix} = \mathbf{T}\begin{bmatrix} I_a \\ I_r \end{bmatrix}. \quad (19)$$

And thus

$$I'_a = \frac{P'}{U_1} = \frac{U_2\sin\delta}{Z} \quad (20)$$

$$I'_r = \frac{Q'}{U_1} = \frac{U_1 - U_2\cos\delta}{Z}. \quad (21)$$

As a variant to the previously described droop method, not the (modified) active and reactive power, but the (modified) active and reactive current I'_a and I'_r are controlled. The frequency and voltage droop control characteristics then become

$$f - f_0 = -k_a(I'_a - I'_{a,0}) = -k_a\frac{X}{Z}(I_a - I_{a,0}) + k_a\frac{R}{Z}(I_r - I_{r,0}) \quad (22)$$

$$U_1 - U_0 = -k_r(I'_r - I'_{r,0}) = -k_r\frac{R}{Z}(I_a - I_{a,0}) - k_r\frac{X}{Z}(I_r - I_{r,0}). \quad (23)$$

This is shown graphically in Fig. 4.

This approach has benefits when U_1 differs significantly from its rated value (e.g., when a short-circuit occurs at U_1, yielding $U_1 = 0$). Implementing (15) and (16) would result in infinitely high currents during the fault, being avoided when (22) and (23) are implemented.

C. Droop Control Through Emulation of a Finite-Output Impedance Voltage Source

An important aspect that must not be overlooked is the supply of harmonic currents, required by non-linear loads. In some island grids, highly non-linear loads incorporating rectifiers, such as ICT equipment and compact fluorescent lamps, may even present the major share of the load. If no adequate strategy is incorporated to supply the harmonics needed for such loads, the voltage quality is severely affected. Unfortunately, the previous approaches do not take possible harmonics into account. Even though the concept of active and reactive power or current is very useful when considering only linear loads, it falls short when considering nonlinear ones. The supply of harmonics to nonlinear loads could be incorporated in two different strategies, either by using a frequency domain approach, thus extending the active and reactive power concept to higher harmonics [9], or by emulating a virtual impedance in the time domain [10]–[13]. Because of its simplicity, the time-domain approach is preferred. In the following of this paper, the active and reactive power concept is abandoned and a purely time-domain approach, obtaining voltage and frequency droop in an alternative way, is developed and implemented.

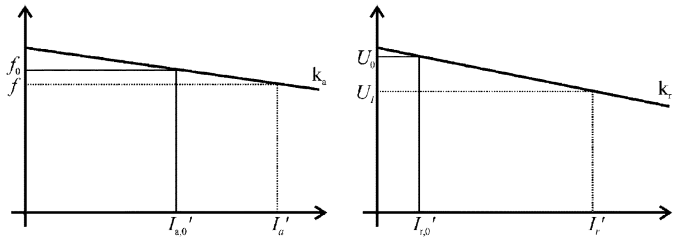

Fig. 4. Frequency and voltage droop characteristics as a function of modified active and reactive power.

Basically, the approach consists of imitating a virtual-system model, shown in Fig. 5(a), consisting of an ac Thévenin equivalent parallel to an ac current source. The Thévenin equivalent consists of an ac voltage source with instantaneous voltage u_{src} in series with a finite-output resistance R_d and inductance L_d. The ac current source has instantaneous current i_{src}. u_{grid} and i_{grid} represent the instantaneous grid voltage and current and correspond to the instantaneous grid voltage and current at the output of the LCL filter of the real system, shown in Fig. 5(b). In the real-system model L_1, R_1, L_2, R_2 and C represent the parameters of the LCL output filter. u_{inv} is the inverter output voltage, i_{inv} the inverter output current and u_{cap} the voltage across the capacitor. For simplicity, these voltages and currents are averaged over the switching period.

The virtual impedance $\underline{Z}_d = R_d + j\omega L_d$ is equivalent to the series impedance of a synchronous generator. However, whereas the series impedance of a synchronous generator is

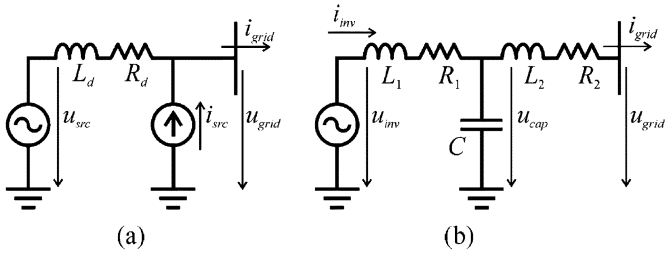

Fig. 5. (a) virtual-system model and (b) real-system model.

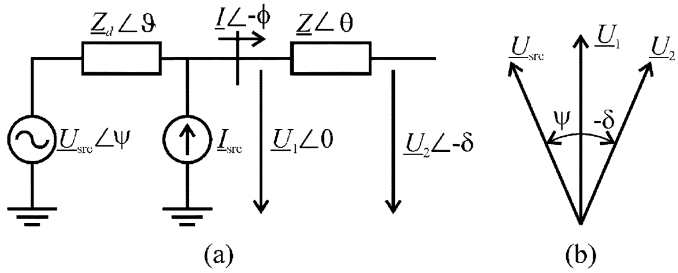

Fig. 6. Virtual-system model in connection with the grid through a line (a) circuit and (b) phasor diagram.

mainly reactive, here the virtual impedance may be chosen arbitrarily. In contrast to a real impedance, this virtual impedance presents no real power losses, and it is thus possible to imitate the behavior of a resistance, without compromising efficiency.

1) Frequency Droop: Both the ac voltage and current source of the virtual-system model are chosen to be purely sinusoidal and may be represented by the phasors $\underline{U}_{\rm src}$ and $\underline{I}_{\rm src}$. Both ac sources are synchronized with the fundamental grid frequency. Frequency droop is obtained as a result of a phase angle difference ψ between $\underline{U}_{\rm src}$ and the fundamental grid voltage component, proportional to the difference between actual (measured) and rated grid frequency

$$\psi = -k_\psi (f - f_0). \tag{24}$$

When the measured grid frequency is lower than the rated grid frequency, the phase angle is positive and $\underline{U}_{\rm src}$ leads the fundamental grid voltage component. When the measured frequency is higher, the phase angle is negative and $\underline{U}_{\rm src}$ lags the fundamental grid voltage component.

2) Voltage Droop: The amplitude $U_{\rm src}$ of the ac voltage source is chosen to be constant and equal to the rated grid voltage amplitude $U_{\rm nom}$. Voltage droop occurs as a result of the difference between instantaneous values of (virtual) $u_{\rm src}$ and (measured) $u_{\rm grid}$, across the series connection of the (virtual) resistance R_d and inductance L_d, causing the current $i_{\rm grid} - i_{\rm src}$ to flow

$$i_{\rm grid} - i_{\rm src} = \frac{1}{R_d + L_d s}(u_{\rm src} - u_{\rm grid}). \tag{25}$$

As this equation involves only instantaneous values, it is a time-domain approach and harmonics are inherently taken into account.

3) ac Current Source as Offset: The ac current source in Fig. 5(a) is added to incorporate an offset active and/or reactive current $\underline{I}_{\rm src}$ generated by the inverter. The combination of the current source with the finite-output impedance voltage source may represent a typical distributed generation (DG) unit (i.e., the current source), with additional frequency and/or voltage regulation capabilities (i.e., the finite-output impedance voltage source). In that case, $i_{\rm src}$ is purely active and relates to the desired active power output of the DG unit. Using this approach, the ancillary service provided by the droop control is seen as an elegant extension of the primary function of a DG unit, i.e., supplying active power [15].

4) Choice of R_d, L_d and k_ψ: Three parameters remain to be chosen, being R_d, L_d, and k_ψ. For a better understanding of their influence, the equivalence is investigated with the previously mentioned droop control method through active and reactive current (Section B). To this purpose, a non-distorted grid is assumed, enabling an analysis using phasors. In Fig. 6, the phasor representation of the virtual-system model is shown. It consists of the ac voltage source $\underline{U}_{\rm src}$ with output impedance $\underline{Z}_d$, in parallel with the current source $\underline{I}_{\rm src}$. The virtual-system model is connected with the grid $\underline{U}_2$ through the line impedance $\underline{Z}$. $\underline{U}_1$ is the voltage at the point of coupling between $\underline{Z}_d$ and $\underline{Z}$.

By analyzing the equivalence of the time-domain approach with the droop control method through active and reactive current, (22) and (23), an appropriate choice of $\underline{Z}_d$ and k_ψ can be made as a function of k_a and k_r. Modified active and reactive current I'_a and I'_r through the point of coupling are

$$\begin{aligned} I_a - jI_r = \underline{I} &= \frac{\underline{U}_{\rm src} - \underline{U}_1}{\underline{Z}_d} + \underline{I}_{\rm src} \\ &= \frac{U_{\rm src}e^{j\psi} - U_1}{Z_d e^{j\vartheta}} + \underline{I}_{\rm src}. \end{aligned} \tag{26}$$

As $Z_d e^{j\theta} = R_d + jX_d$

$$\begin{aligned} &I_a - I_{a,{\rm src}} \\ &\quad = \frac{R_d(U_{\rm src}\cos\psi - U_1) + X_d U_{\rm src}\sin\psi}{Z_d^2} \end{aligned} \tag{27}$$

$$\begin{aligned} &I_r - I_{r,{\rm src}} \\ &\quad = \frac{-R_d U_{\rm src}\sin\psi + X_d(U_{\rm src}\cos\psi - U_1)}{Z_d^2}. \end{aligned} \tag{28}$$

If $\vartheta = \theta$, i.e., $R_d/X_d = R/X$, transformation by $\mathbf{T}$ yields

$$I'_a - I'_{a,{\rm src}} = \frac{U_{\rm src}\sin\psi}{Z_d} \tag{29}$$

$$I'_r - I'_{r,{\rm src}} = \frac{U_{\rm src}\cos\psi - U_1}{Z_d}. \tag{30}$$

Based on (22), (23), (24), (29), and (30), and assuming that $\sin\psi \cong \psi$ and $\cos\psi \cong 1$, the following equations for Z_d and k_ψ as a function of k_a and k_r hold

$$Z_d = k_r \tag{31}$$

$$k_\psi = \frac{k_r}{U_{\rm src}k_a}. \tag{32}$$

A good strategy in determining $\underline{Z}_d$ and k_ψ, is therefore to obtain the desired k_a and k_r from Fig. 4, then to calculate Z_d and k_ψ from (31) and (32). The ratio R_d/X_d should be chosen

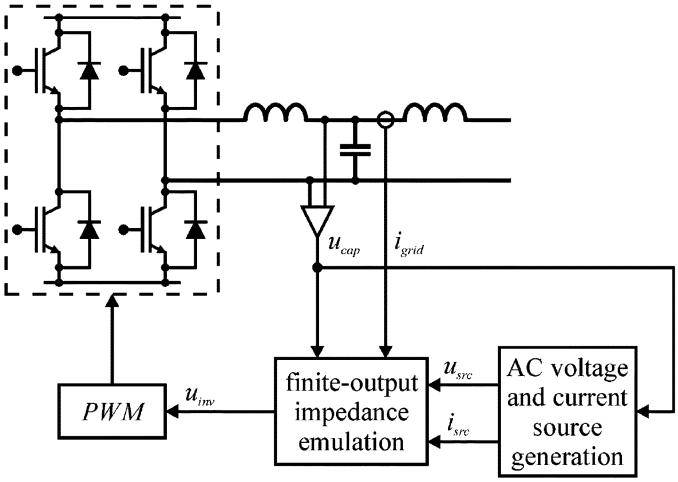

Fig. 7. Overall scheme for the proposed voltage and frequency droop control method.

equal to the R over X ratio of the line impedance, as then the control of voltage amplitude and frequency are decoupled (see Fig. 3), ensuring the most "efficient" control of both amplitude and frequency relative to the supplied current.

From this analysis, it can be concluded that the approach of imitating a finite-output impedance voltage source, is equivalent to the droop control through controlling modified active and reactive current, except for the additional benefit of intrinsically controlling as well the voltage harmonics through a droop characteristic. Compared to the classical droop control method through controlling active and reactive power, the approach exhibits, in addition to the voltage harmonics mitigation, benefits regarding short-circuit behavior and achieves (in the case of a non-negligible line resistance) a more "efficient" control of frequency and voltage.

III. Implementation

The purpose of the control scheme is to emulate the behavior described in Section II.C by controlling current and voltage output of a single-phase PWM voltage source inverter with LCL output filter. In Fig. 5 both the virtual-system model of the finite-output impedance voltage source and the real-system model of the LCL output filter are shown. The output current i_{grid} and voltage u_{grid} are measured, whereas the grid parameters on the right hand of the bar are unknown. This unknown grid may be an infinite bus, a microgrid, or a stand-alone load, meaning that the grid impedance may range from almost zero (infinite bus) up to infinity (no-load stand-alone). The control scheme should be able to control u_{grid} and i_{grid}, emulating the virtual-system model, irrespective of the grid impedance. For practical reasons, in the subsequent development, capacitance voltage u_{cap} and i_{grid} instead of grid voltage u_{grid} and i_{grid} of the real-system model are controlled to be equal to u_{grid} and i_{grid} of the virtual-system model.

The overall control scheme, implementing the proposed voltage and frequency droop control method, is shown in Fig. 7. The control scheme is decomposed in two main parts. The rightmost generates the virtual-system voltage source u_{src} and current source i_{src} by tracking the fundamental amplitude and frequency of the voltage u_{cap} and applying the phase shift ψ according to (24). The second part emulates the finite-output impedance, by calculating the inverter voltage u_{inv} that should be applied by PWM to the real system, based on the virtual-system voltage source u_{src} and current source i_{src} and measured values u_{cap} and i_{grid}. The implementation of both parts is specified in the next subsections.

A. Voltage and Current Source Generation

Error! Reference source not found. presents the full scheme to generate the reference voltage u_{src} and current i_{src}, using only the measured value of u_{cap}. This scheme comprises two subparts, the first achieving fundamental voltage amplitude and frequency tracking, the second calculating the phase shift and amplitude of voltage u_{src} and current i_{src}.

1) Fundamental Voltage Amplitude and Frequency Tracking: Based on a single-phase grid voltage measurement u_{cap}, the fundamental voltage amplitude U_{grid} and frequency f_{grid} are estimated. To this purpose, the fundamental voltage is extracted by use of a Kalman estimator. The approach is based on a technique, described in literature, where it is used for voltage harmonics tracking [16]. The Kalman estimator observes, besides the fundamental component, also the 3rd, 5th, and 7th harmonic components. Observing these harmonics improves the tracking performance under distorted voltage conditions considerably. The fundamental output component is used further, represented by two values u_α and u_β, the former being in phase with u_{cap}, the latter representing the quadrature component. These components are named u_α and u_β, as they are equivalent to the components from Clark's transformation in a three-phase system. Subsequently, Park's transformation is applied, resulting in u_d and u_q. The rotation angle θ for Park's transformation is obtained from a phase locked loop (PLL), regulating u_q to zero by use of a proportional-integral (PI) regulator [17]. As a result, u_d is equal to the amplitude U_{grid} of the fundamental voltage, whereas the frequency f_{grid} is a result from inside the PLL (Fig. 8). In Fig. 9, the fundamental voltage and frequency tracking of a distorted voltage waveform is illustrated by a simulation. The fundamental voltage is tracked in about 5 periods, whereas the initial errors in u_d and u_q due to an initial phase shift of $\pi/2$ decay in about 8 periods.

2) Phase Shift and Amplitude Calculation: Based on the estimated fundamental voltage amplitude U_{grid} and frequency f_{grid}, the amplitude U_{src} and the power angle ψ of the virtual-system voltage source u_{src} are

$$\psi = -k_\psi (f - f_0) \tag{33}$$

$$U_{\mathrm{src}} = U_0. \tag{34}$$

Equations (33) and (34) are adjusted to account (approximately) for the limited current rating $I_{\max}$ of the inverter by ensuring that (not shown in Fig. 8)

$$U_{\mathrm{grid}} - \|Z_d\| I_{\max} \leqslant U_{\mathrm{src}} \leqslant U_{\mathrm{grid}} + \|Z_d\| I_{\max} \tag{35}$$

$$\|\psi\| \leqslant \min\left(\frac{\pi}{2}, \frac{\|Z_d\| I_{\max}}{U_0}\right). \tag{36}$$

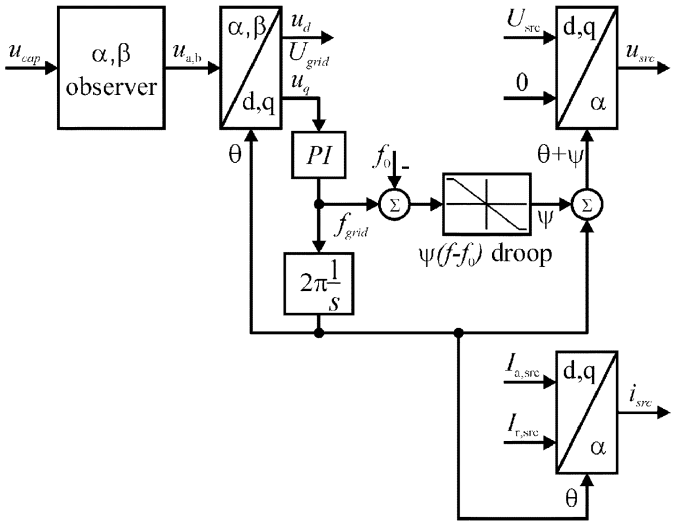

Fig. 8. Voltage and current source generation scheme.

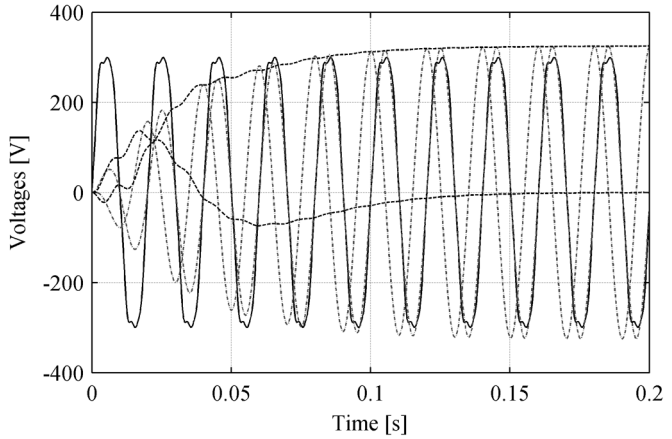

Fig. 9. Fundamental voltage and amplitude tracking: $u_{\rm cap}$ (black solid), u_α and u_β (gray dash-dotted), u_d and u_q (black dashed).

Applying inverse Park's transformation on $[U_{\rm src}0]$ with the rotation angle $\theta+\psi$ returns the sinusoidal voltage $u_{\rm src}$.

B. Finite-Output Impedance Emulation

The emulation of the finite-output impedance is obtained by the use of a mixed voltage-current controller. Instead of having a primary current control loop for $i_{\rm grid}$ inside a secondary voltage control loop for $u_{\rm cap}$ (or the other way round), both current and voltage are simultaneously controlled, emulating the finite-output impedance. This approach is necessary as the grid impedance is not known, and may vary from 0 to ∞. Stability problems would arise in a primary current control loop for very large grid impedances, whereas the same is true in a primary voltage control loop for very small grid impedances (see, e.g., [2]). Different control methods can be used hereto, such as classical (e.g., root locus), modern [e.g., linear quadratic gaussian (LQG)], robust (e.g., $\rm H_\infty$) or non-linear (e.g., adaptive) control methods. Here, the LQG optimal control approach is followed, using a Kalman estimator and a linear quadratic regulator.

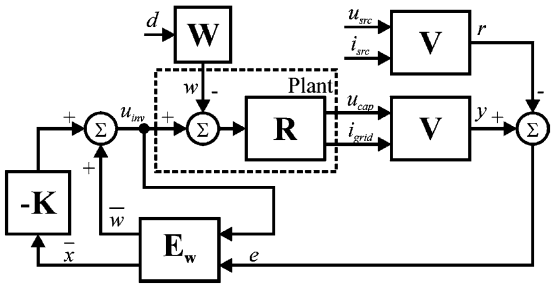

Fig. 10. LQG control scheme for the finite-output impedance emulation.

The control scheme is shown in Fig. 10 and incorporates disturbance estimation as well as reference following [18]. The real-system plant model $\mathbf{R}$ is described in state-space domain by

$$
\begin{aligned}
s\begin{bmatrix} i_{\rm inv} \\ u_{\rm cap} \\ i_{\rm grid} \end{bmatrix} &= \begin{bmatrix} -\frac{R_1}{L_1} & -\frac{1}{L_1} & 0 \\ \frac{1}{C} & 0 & -\frac{1}{C} \\ 0 & \frac{1}{L_2} & -\frac{R_2}{L_2} \end{bmatrix} \begin{bmatrix} i_{\rm inv} \\ u_{\rm cap} \\ i_{\rm grid} \end{bmatrix} \\
&\quad + \begin{bmatrix} \frac{1}{L_1} \\ 0 \\ 0 \end{bmatrix} [u_{\rm inv} + w] \\
\begin{bmatrix} u_{\rm cap} \\ i_{\rm grid} \end{bmatrix} &= \begin{bmatrix} 0 & 1 & 0 \\ 0 & 0 & 1 \end{bmatrix} \begin{bmatrix} i_{\rm inv} \\ u_{\rm cap} \\ i_{\rm grid} \end{bmatrix} \\
&\quad + \begin{bmatrix} 0 \\ 0 \end{bmatrix} [u_{\rm inv} + w]. \qquad (37)
\end{aligned}
$$

Whereas in [19] the grid voltage $u_{\rm grid}$ is an explicit input of the system, in (37) $u_{\rm grid}$ is incorporated in the input-equivalent disturbance w, caused by the combination of the grid voltage $u_{\rm grid}$ and the reference signal $u_{\rm src}$ and $i_{\rm src}$. In fact, w is a virtual signal applied at the control input, producing the same steady state error e (Fig. 10) as the combination of the actual disturbance $u_{\rm grid}$ and the reference signals $u_{\rm src}$ and $i_{\rm src}$. Both disturbances are persistent, as they are both composed of sinusoidal components. These persistent disturbances are modelled and nullified. $\mathbf{W}$ represents the input-equivalent disturbance model, with d an arbitrary impulse input. Besides the fundamental component, also the 3rd, 5th, 7th, 9th, 11th, and 13th harmonic components are modelled.

The virtual-system model is incorporated through the transfer function $\mathbf{V}$:

$$e = \frac{Z_d}{Z_d+Z_b}\frac{u_{\rm cap}-u_{\rm src}}{L_d s+R_d} + \frac{Z_d}{Z_d+Z_b}(i_{\rm grid}-i_{\rm src}). \qquad (38)$$

The output e represents the error on the desired behavior (25). The error is normalized through $Z_d/(Z_d+Z_b)$. Z_b is an arbitrary base impedance, e.g., chosen equal to the LCL filter impedance $Z_1 = R_1+\omega L_1$. Although not strictly necessary, this normalization enables the use of virtual output impedances ranging from 0 to infinity. Zero virtual output impedance results in a voltage controller, whereas infinite output impedance corresponds to a current controller. Any non-zero finite output impedance results in a mixed current-voltage controller. In this sense, the approach is to be considered as a generalization of the current controller [19], to a mixed current-voltage controller.

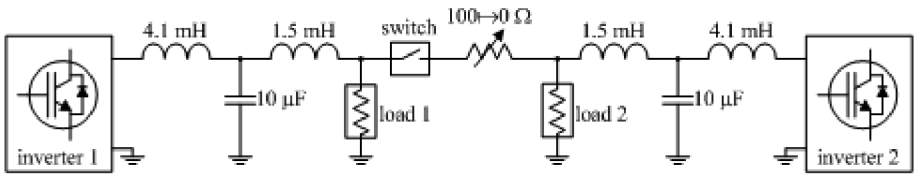

Fig. 11. Scheme of the experimental setup comprising two parallel-connected inverters, the LCL filters, loads and switch.

The Kalman estimator $\mathbf{E_w}$ estimates the states as well as the input-equivalent disturbance, nullified at the plant input u_{inv}. The estimator is obtained by calculating the Kalman filter for the real-system plant model $\mathbf{R}$, augmented with $\mathbf{V}$ and $\mathbf{W}$, using the SATLAB function kalman.m.

The control law $\mathbf{K}$ is obtained by calculating the LQG optimal state-feedback gain of the real system model $\mathbf{R}$, augmented only by $\mathbf{V}$ ($\mathbf{W}$ is not controllable), using the MATLAB function dlqr.m. The inverter voltage u_{inv} is obtained by augmenting the output of the control law with the estimate of the input-equivalent disturbance.

IV. EXPERIMENTAL RESULTS

The control algorithm is converted from MATLAB/Simulink to "C"-code using Real-Time Workshop. The code is then executed on a Texas Instruments C6711 digital signal processor (DSP). An FPGA daughter card on top of the C6711 DSK board generates the PWM signals for the IGBT PWM voltage-source inverter and provides an interface to the voltage and current measurements [20], [21]. The total processor load is 81% with the algorithm running at 9.2 kHz, being equal to and synchronized with the switching frequency of the inverter.

Using the set-up (Fig. 11), experiments have shown the performance of the technique for resistive, inductive and capacitive loads and compact fluorescent lamps, the latter drawing a highly non-linear current. Also good results are obtained, during short-circuits and connection to the main grid. A second identical inverter set-up is added to test the performance during parallel operation of two inverters.

Both inverters have a power rating of about 2.5 kW. In the experimental set-up, the LCL PWM filter values are: $L_1 = 4.1$ mH, $L_2 = 1.5$ mH, $C = 10$ μF. The parasitic (series) resistances associated with both inductances of the LCL filter are $R_1 = 0.95$ Ω and $R_2 = 1$ Ω, respectively. Note that though the parasitic resistances of the LCL circuit are relatively large, the system is still underdamped. It is the merit of the LQR controller that this underdamped circuit is accurately controlled as it inherently provides active damping to the system. This is even more valuable at higher power levels, where parasitic resistances are much smaller to prevent the occurrence of excessive power losses.

As a first example, demonstrating the steady-state behavior of the virtual impedance droop method, the supply of a highly nonlinear load is considered for two different ohmic droop impedances. A single inverter is operated in island, with the load consisting of eight compact fluorescent lamps of different ratings. In Fig. 12, the virtual droop impedance is chosen equal to 1 Ω purely ohmic, whereas in Fig. 13, the virtual impedance is

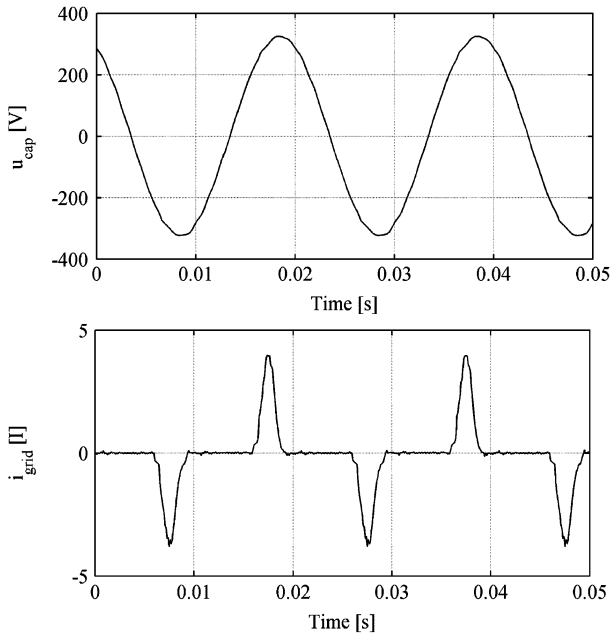

Fig. 12. Voltage and current waveforms feeding a highly nonlinear load with $Z_d = 1$ Ω ohmic.

10 Ω, also purely ohmic. The resulting voltage total harmonic distortion is 0.5% and 3.6%, respectively.

In a second example, two stand-alone grids are constructed, each consisting of one inverter supplying a resistive load (Fig. 11). The experiment shows the parallel connection of both grids. The connection is obtained by first placing a 100 Ω resistance between both stand-alone grids, and gradually reducing this resistance in one second to 0 Ω. Fig. 14 shows the grid voltages and currents of both inverters during connection. The close-up graphs show the voltages and currents as they were registered shortly before and after connection. It can be seen that the voltages synchronize smoothly, while the currents stabilize after a modest transient to almost perfect load sharing. Here, the droop impedance is chosen to be equal to 5 Ω, with a ratio $R_d/X_d = 4$, and $k_\psi = 1$ rad/Hz.

Fig. 15 shows the difference between voltage and current outputs of both inverters during the experiment. It clearly shows the time of connection at about 0.23 s through the 100 Ω impedance which is gradually reduced until it reaches zero at about 1.0 s, at which time both voltages are equal. In the meantime, the current difference increased and only from 1.0 s on it decreases gradually to disappear almost completely at about 2.0 s. If both inverters were instantaneously connected with each other, convergence would have been slightly faster, though accompanied

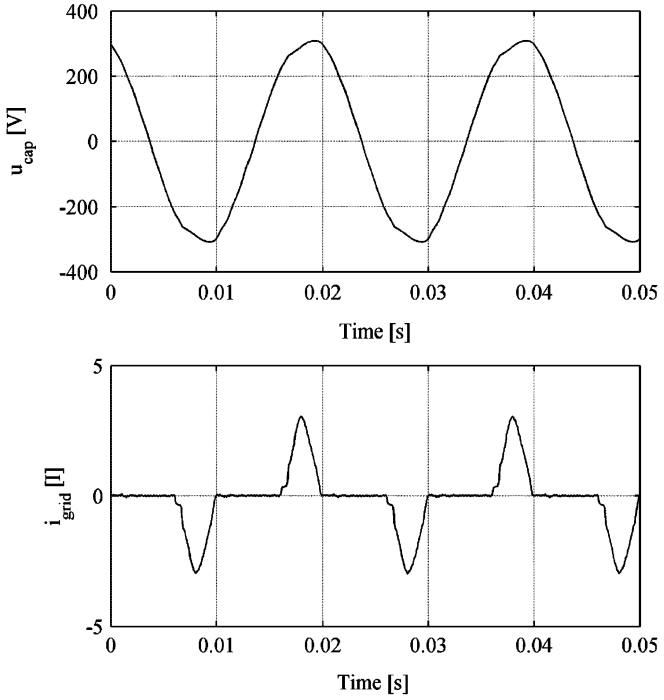

Fig. 13. Voltage and current waveforms feeding a highly nonlinear load with $Z_d = 10\ \Omega$ ohmic.

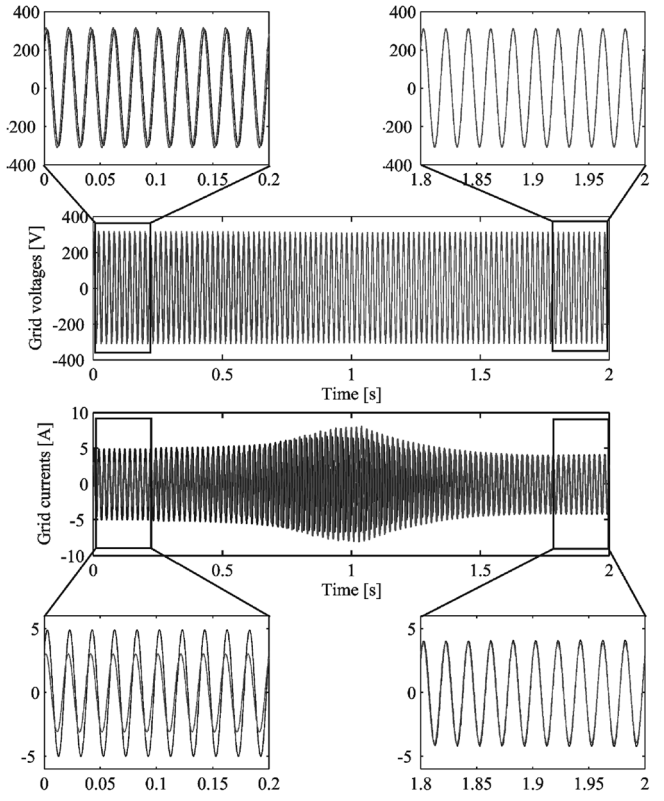

Fig. 14. Experimental grid currents and voltages before, during and after the connection of two non-synchronized stand-alone grids.

with higher transient currents. Therefore, instantaneous connection is only practical when both inverters are synchronized *before* connection.

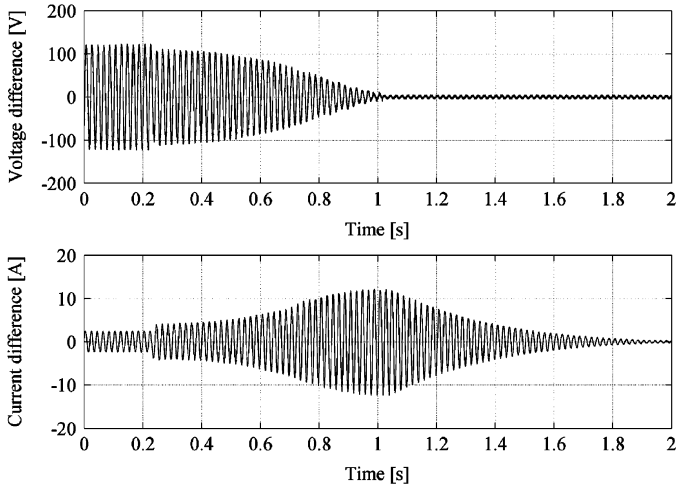

Fig. 15. Difference between voltage and current outputs of both inverters before, during and after connection.

V. Conclusion

A time-domain method for controlling voltage and frequency using parallel inverters connected to the mains or in an island grid is developed. By imitating a voltage source with a complex finite-output impedance, voltage droop control is obtained. Frequency droop control results from synchronizing the power source with the grid, with a phase angle difference that depends on the difference between rated and actual grid frequency. Compared to existing techniques, the described method exhibits superior behavior, considering the mitigation of voltage harmonics, the behavior during short-circuit and, in the case of a non-negligible line resistance, the "efficient" control of frequency and voltage. Two experiments are included to show the described behavior.

References

[1] A. Tuladhar, H. Jin, T. Unger, and K. Mauch, "Parallel operation of single phase inverter modules with no control interconnections," in *Proc. IEEE-APEC'97 Conf.*, Feb. 23–27, 1997, vol. 1, pp. 94–100.

[2] E. A. A. Coelho, P. C. Cortizo, and P. F. D. Garcia, "Small-signal stability for parallel-connected inverters in stand-alone AC supply systems," *IEEE Trans. Ind. Appl.*, vol. 38, no. 2, pp. 533–542, Mar./Apr. 2002.

[3] M. C. Chandorkar, D. M. Divan, and R. Adapa, "Control of parallel connected inverters in standalone AC supply systems," *IEEE Trans. Ind. Appl.*, vol. 29, no. 1, pp. 136–143, Jan./Feb. 1993.

[4] A. Engler, "Regelung von Batteriestromrichtern in modularen und erweiterbaren Inselnetzen," Ph.D. dissertation, Dept. Elect. Eng., Univ. Gesamthochschule Kassel, Kassel, Germany, 2001.

[5] M. Hauck and H. Späth, "Control of three phase inverter feeding an unbalanced load and operating in parallel with other power sources," in *Proc. EPE-PEMC'02 Conf.*, Sep. 9–11, 2002.

[6] C.-C. Hua, K.-A. Liao, and J.-R. Lin, "Parallel operation of inverters for distributed photovoltaic power supply system," in *Proc. IEEE-PESC'02 Conf.*, Jun. 23–27, 2002, pp. 1979–1983.

[7] D. Shanxu, M. Yu, X. Jian, K. Yong, and C. Jian, "Parallel operation control technique of voltage source inverters in UPS," in *Proc. IEEE PEDS'99 Conf.*, Jul. 27–29, 1999, pp. 883–887.

[8] K. Wallace and G. Mantov, "Wireless load sharing of single phase telecom inverters," in *Proc. IEEE INTELEC'99 Conf.*, Jun. 6–9, 1999, CD-ROM.

[9] U. Borup, F. Blaabjerg, and P. N. Enjeti, "Sharing of nonlinear load in parallel-connected three-phase converters," *IEEE Trans. Ind. Appl.*, vol. 37, no. 6, pp. 1817–1823, Nov./Dec. 2001.

[10] S. J. Chiang and J. M. Chang, "Parallel control of the UPS inverters with frequency-dependent droop scheme," in *Proc. IEEE PESC'01 Conf.*, Jun. 17–21, 2001, pp. 957–961.
[11] T. Skjellnes, A. Skjellnes, and L. E. Norum, "Load sharing for parallel inverters without communication," in *Proc. NORPIE'02 Conf.*, Aug. 12–14, 2002.
[12] L. Mihalache, "Paralleling control technique with no intercommunication signals for resonant controller-based inverters," in *Proc. IEEE IAS'03 Annu. Meeting*, Oct. 12–16, 2003, vol. 3, pp. 1882–1889.
[13] J. M. Guerrero, L. G. de Vicuña, J. Matas, J. Miret, and M. Castilla, "A wireless load sharing controller to improve dynamic performance of parallel-connected UPS inverters," in *Proc. IEEE PESC'03 Conf.*, Jun. 15–19, 2003, pp. 1408–1413.
[14] B. M. Weedy and B. J. Cory, *Electric Power Systems*, 4th ed. New York: Wiley, 1998.
[15] K. De Brabandere, A. Woyte, R. Belmans, and J. Nijs, "Prevention of inverter voltage tripping in high density PV grids," in *Proc. EU-PVSEC'04 Conf.*, Jun. 7–11, 2004.
[16] A. A. Girgis, W. B. Chang, and E. B. Makram, "A digital recursive measurement scheme for on-line tracking of power system harmonics," *IEEE Trans. Power Del.*, vol. 6, no. 3, pp. 1153–1160, Jul. 1991.
[17] V. Kaura and V. Blasko, "Operation of a phase locked loop system under distorted utility conditions," in *Proc. IEEE-APEC'96 Conf.*, Mar. 3–7, 1996, vol. 2, pp. 703–708.
[18] G. F. Franklin, J. D. Powell, and M. Workman, *Digital Control of Dynamic Systems*, 3rd ed. Menlo Park, CA: Addison Wesley Longman, 1998.
[19] B. Bolsens, K. De Brabandere, J. Van de Keybus, J. Driesen, and R. Belmans, "Model-based generation of low distortion currents in grid-coupled PWM-inverters using an LCL output filter," in *Proc. IEEE PESC'04 Conf.*, Jun. 20–25, 2004, pp. 4616–4622.
[20] J. Van de Keybus, "Development of a universal power measurement and control platform for low-voltage grid-coupled applications in a deregulated electricity market," Ph.D. dissertation, K.U. Leuven, Leuven, Dec. 2003.
[21] J. Van den Keybus, K. De Brabandere, B. Bolsens, and J. Driesen, "Using a fully digital rapid prototype platform in grid-coupled power electronics applications," in *Proc. IEEE COMPEL'04 Conf.*, Aug. 15–18, 2004.

Karel De Brabandere (S'05) received the M.Sc. degree in electrotechnical engineering from the Katholieke Universiteit Leuven, Leuven, Belgium, in 2000, where he is currently pursuing the Ph.D. degree on the subject of the control of grid-connected power electronic inverters for the integration of distributed energy resources in island grids and the utility grid.

His research interests include power electronics, digital control, distributed power systems and microgrids.

Bruno Bolsens (S'03) received the M.Sc. degree in electrotechnical engineering from the Katholieke Universiteit Leuven, Leuven, Belgium, in 2000, where he is currently pursuing the Ph.D. degree on the subject of power electronic circuits with limited electromagnetic interference properties in electric distribution networks.

His research interests include power electronics, digital control, inverter topologies, power quality and EMC issues.

Jeroen Van den Keybus (S'05) was born in Belgium in 1975. He graduated in electrical engineering and received the Ph.D. degree from the Katholieke Universiteit Leuven (K.U. Leuven), Leuven, Belgium, in 1998 and 2003, respectively.

He is currently a Research Assistant at the K.U. Leuven—ESAT department where he performs research in the area of power electronics, and has a wide working knowledge and expertise in designing complex digital systems using reconfigurable and dedicated signal processing components.

Achim Woyte received the electrical engineering degree from the University of Hannover, Hannover, Germany, in 1997 and the Ph.D. degree in engineering from the Katholieke Universiteit Leuven (K.U. Leuven), Leuven, Belgium, in 2003.

At the beginning of 2004, he joined the Policy Studies Department of the Brussels-based consultant company, 3E. There, he coordinates policy-related projects in renewable energy technology. He also performs research and engineering regarding the integration of electricity from renewable sources into power systems and markets. He is the coauthor of more than 50 scientific publications.

Johan Driesen (S'93–M'97) was born in Belgium in 1973. He received the M.Sc. degree in electrotechnical engineering and the Ph.D. degree in electrical engineering (on the subject of finite element solution of coupled thermal-electromagnetic problems and related applications in electrical machines and drives, microsystems and power quality issues) from the Katholieke Universiteit Leuven (K.U. Leuven), Leuven, Belgium, in 1996 and 2000, respectively.

Currently, he is an Associate Professor at K.U. Leuven and teaches power electronics and drives. In 2000–2001 he was a Visiting Researcher in the Imperial College of Science, Technology and Medicine, London, U.K. In 2002, he was with the University of California, Berkeley. Currently he conducts research on distributed generation, including renewable energy systems, power electronics and its applications, for instance in drives and power quality.

Ronnie Belmans (S'77–M'84–SM'89–F'05) received the M.Sc. degree in electrical engineering and the Ph.D. degree from the Katholieke Universiteit Leuven (K.U. Leuven), Leuven, Belgium, in 1979 and in 1984, respectively, and the Special Doctorate and the Habilitierung both from the RWTH, Aachen, Germany, in 1989 and 1993, respectively.

Currently, he is a Full Professor with K.U. Leuven, where he teaches electric power and energy systems. His research interests include techno-economic aspects of power systems, power quality and distributed generation. He is also a Guest Professor at Imperial College of Science, Medicine and Technology, London, U.K.

Dr. Belmans has been the Chairman of the Board of Directors of ELIA, the Belgian transmission grid operator, since June 2002.